minerals

MDPI

Communication

Bi-Ag-Sulfosalts and Sulfoarsenides in the Ruwai Zn-Pb-Ag Skarn Deposit, Central Borneo, Indonesia

Cendi D. P. Dana [1,2,*], Andrea Agangi [2], Arifudin Idrus [3], Chun-Kit Lai [4] and Doly R. Simbolon [5]

1 Earth and Planetary Science Institute, School of GeoSciences, The University of Edinburgh, Edinburgh EH9 3FE, UK
2 Graduate School of International Resource Sciences, Akita University, Akita 010-0852, Japan
3 Department of Geological Engineering, Universitas Gadjah Mada, Yogyakarta 55281, Indonesia
4 Fortescue Metals Group Ltd., East Perth, WA 6004, Australia
5 PT Kapuas Prima Coal, Tbk., North Jakarta 14460, Indonesia
* Correspondence: c.d.p.dana@sms.ed.ac.uk

Abstract: The Ruwai skarn deposit is located in the Schwaner Mountain complex within the central Borneo gold belt and is currently considered the largest Zn skarn deposit in Indonesia. The deposit has been known to host Zn-Pb-Ag mineralization in the form of massive sulfide ore bodies; however, the occurrence of Ag-bearing minerals has not been identified yet. This study documents the mineralogical characteristics of several Bi-Ag sulfosalts and sulfoarsenides, as well as their chemical compositions. Ten Bi-Ag sulfosalts were identified, including native bismuth, tetrahedrite, cossalite, tsumoite, bismuthinite, joseite-B, Bi_6Te_2S, Bi-Pb-Te-S, Bi-Ag-S, and Bi-Te-Ag. Three sulfoarsenides were identified, including arsenopyrite, glaucodot, and alloclasite. The occurrence of Bi-Ag sulfosalts is typically associated with massive sulfide mineralization, although tsumoite can also be found associated with massive magnetite. In terms of sulfoarsenides, both arsenopyrite and glaucodot are associated with massive sulfide mineralization, whereas alloclasite is associated with massive magnetite mineralization. The Bi-bearing minerals are characterized by irregular, bleb-like texture or patch morphology, and occur either as free grains or inclusions within sulfides, such as galena or pyrite. Tetrahedrite typically has an anhedral shape with a rim or atoll texture surrounding sphalerite or galena. In contrast, sulfoarsenides are typically found as euhedral–subhedral grains where glaucodot typically is rimmed by arsenopyrite. Both Bi-Ag sulfosalt and sulfoarsenides were formed during the retrograde stage under high oxidation and a low sulfidation state condition. The ore-forming temperature based on arsenopyrite geothermometry ranges from 428 °C to 493 °C.

Keywords: Ruwai; skarn; sulfosalts; bismuth; silver; arsenides; Borneo

Citation: Dana, C.D.P.; Agangi, A.; Idrus, A.; Lai, C.-K.; Simbolon, D.R. Bi-Ag-Sulfosalts and Sulfoarsenides in the Ruwai Zn-Pb-Ag Skarn Deposit, Central Borneo, Indonesia. *Minerals* **2022**, *12*, 1564. https://doi.org/10.3390/min12121564

Academic Editors: Majid Ghaderi, Huan Li and Kotaro Yonezu

Received: 10 November 2022
Accepted: 30 November 2022
Published: 4 December 2022

1. Introduction

The Ruwai skarn deposit is one of the few Zn-Pb skarn deposits in Indonesia, along with Tuboh on Sumatra Island and Gunung Malang on Java Island [1–3]. The recent resource estimation indicates a total resource of up to 14.43 Mt at 4.94% Zn; 3.28% Pb; 108.11 g/t Ag [4], which identifies Ruwai as the largest zinc skarn deposit in Indonesia. The Ruwai skarn deposit was discovered in 1918 by a Dutch investigation program and is currently under the management of PT Kapuas Prima Coal, Tbk. Several previous studies mentioned that this deposit is enriched in Ag and Bi [5–7]; however, silver and bismuth minerals have not been reported so far. This study presents the first detailed account of the occurrence and chemical compositions of several Bi-Ag sulfosalts and sulfoarsenides in the Ruwai skarn deposit, which implies a better understanding of their ore-forming conditions.

2. Geological Background

The Ruwai skarn deposit is located within the Central Borneo gold belt in the Schwaner Mountains (Figure 1) (modified after [8]). The oldest stratigraphic unit in this area consists

of volcanic facies (part of the top of the Triassic Kuayan Formation), overlying the older Jurassic Ketapang Complex consisting of limestone, siltstone, and sandstone (Figure 2) [6,9,10]. Most of the skarn mineralization at Ruwai is hosted in the limestone unit of the Ketapang Complex [5,6]. The intrusions in this area belong to the Cretaceous Sukadana Granitoids [5,6,11]. At least three types of intrusions are found including intermediate, felsic, and mafic dykes, where the felsic and intermediate intrusions are interpreted to be the syn-mineralization intrusion, whereas the mafic dykes intruded post-mineralization [6,11]. In terms of the structural framework, NNW-SSE, NW-SE, and WSW-ENE lineaments dominate the studied area [6]. A magnetic and VLF survey showed two major faults, a NNE sinistral strike-slip fault zone, and an ENE normal fault zone [12].

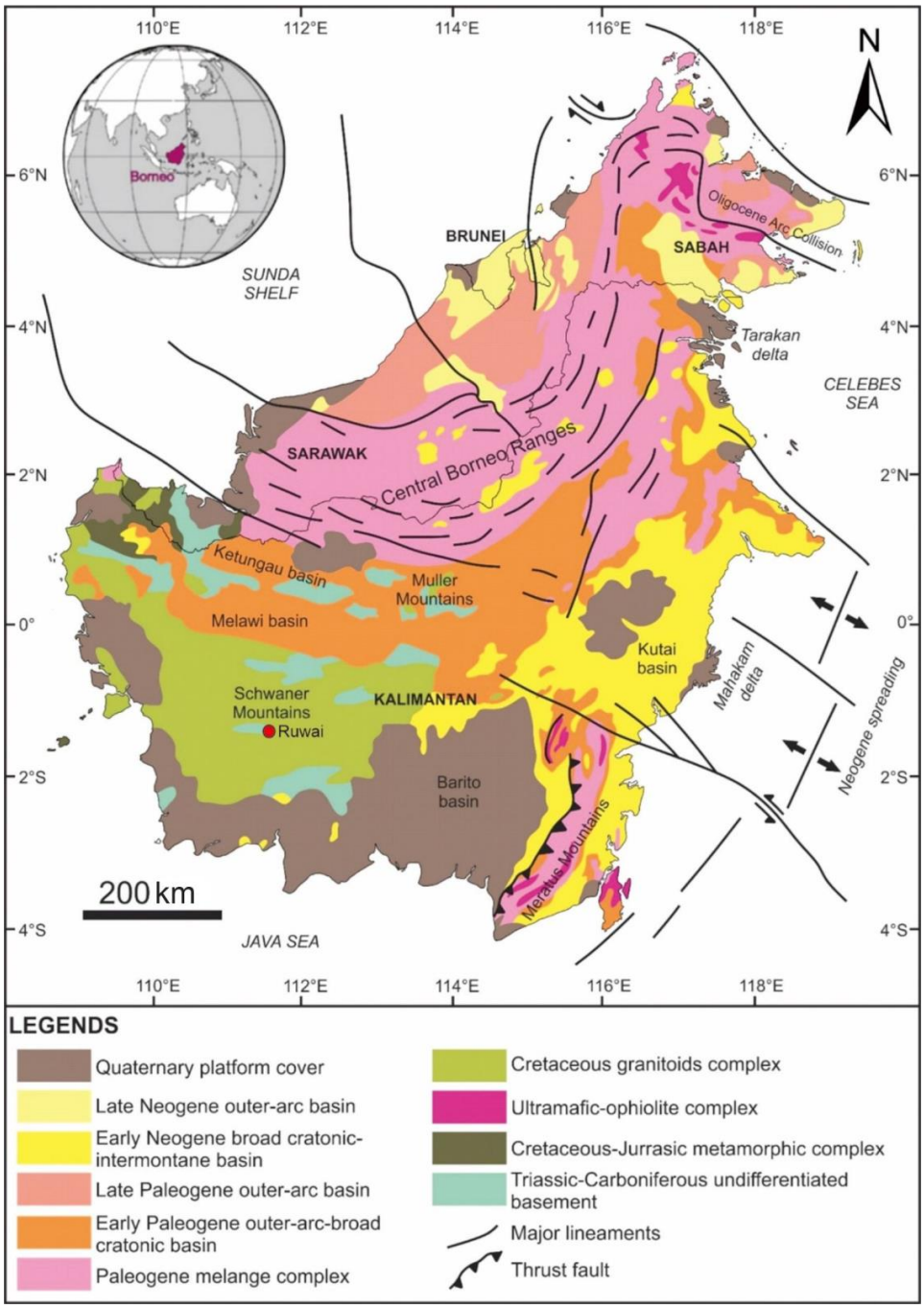

Figure 1. Regional physiography and geological framework of Borneo island where the Ruwai skarn deposit is located within Schwaner Mountains complex in the southwestern part of the island.

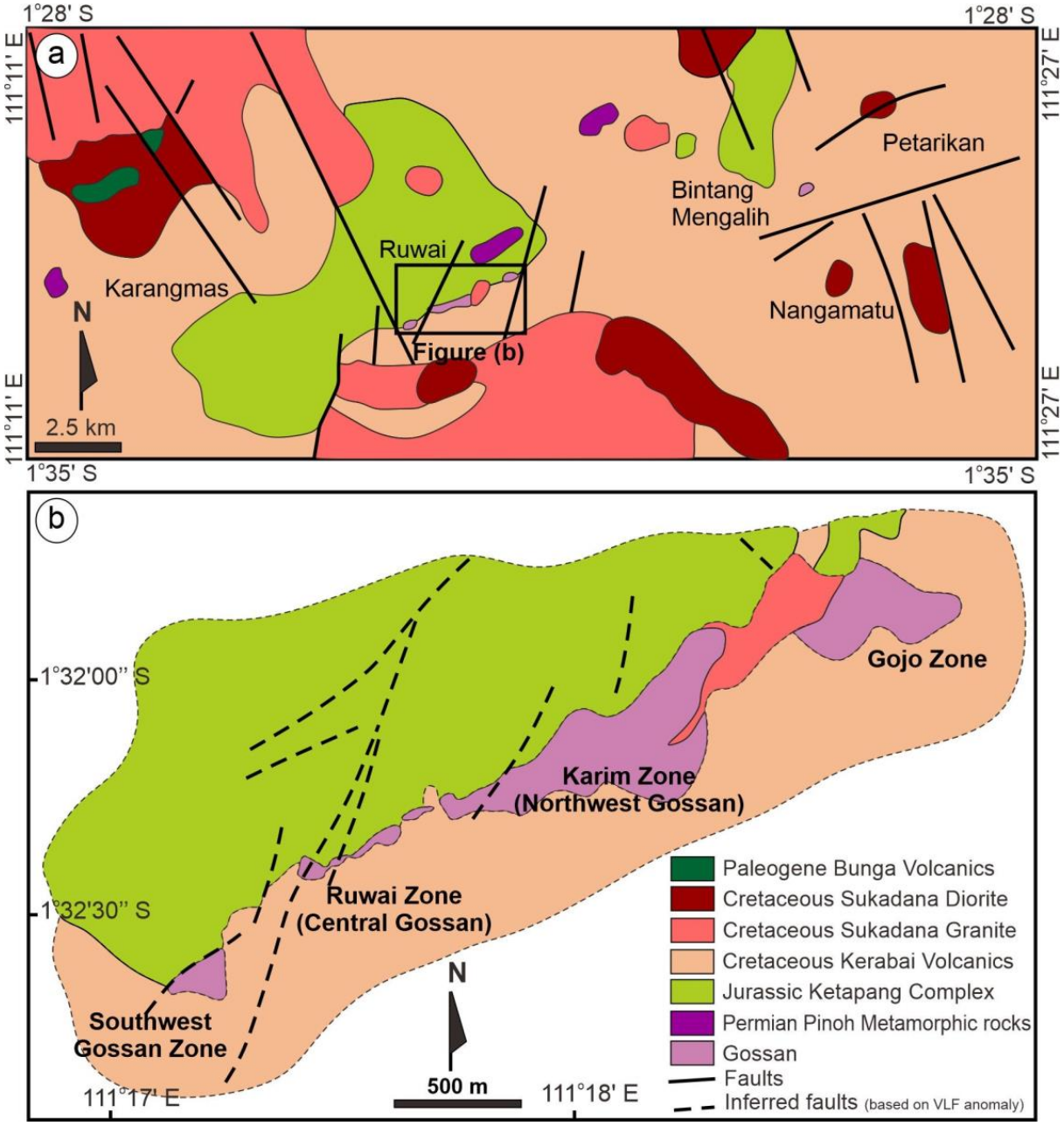

Figure 2. Simplified regional (**a**) and local (**b**) geological map of the Ruwai skarn deposit (modified after [6,9,10]).

The formation of the Ruwai skarn deposit can be divided into three main stages, including prograde, retrograde, and supergene stages. Garnet and pyroxene predominantly occur in the prograde stage whereas epidote–chlorite–actinolite are abundant in the retrograde stage. The initial mineralization of Fe- minerals, such as pyrite, magnetite, and chalcopyrite occurred in the prograde stage, whilst the formation of massive ore bodies (i.e., massive sulfides and magnetite) took place in the retrograde phase (Figure 3). Those mineral assemblages then went into the supergene alteration as characterized by the formation of metal-bearing hydrous minerals, such as chalcanthite and hemimorphite. Most of the mineralization at Ruwai is developed in mantos at the contact between siltstone (upper strata) and limestone (lower strata) and within the limestone itself as the favorable host rock. The mineralization is spatially related to small stocks and dykes that are believed to originate from the main intrusive center [6,10]. Minor disseminated base metal

mineralization is usually found in the prograde skarn, with drill hole assays being in the range of 1–5% Pb+Zn and less than 50 g/t Ag [6]. Outward from the prograde skarn, the retrograde skarn shows significant grades of base metals of up to 10% Pb+Zn and 100 g/t Ag occurring in disseminated form and veins or veinlets [6]. The main mineralization zone is developed in massive sulfide bodies with high grades of up to 30% Pb+Zn and 1000 g/t Ag [6,7]. Massive sulfide bodies tend to occur enveloped in retrograde skarn and at the contact of siltstone and limestone, similar to many other Zn-Pb skarns worldwide [13,14].

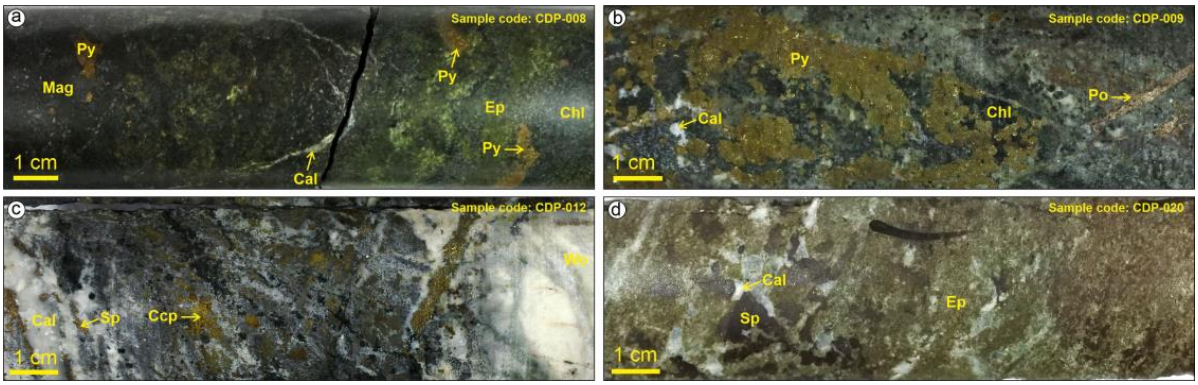

Figure 3. Representative drill core samples from Ruwai: (**a**) massive magnetite–epidote skarn; (**b**) disseminated pyrite-pyrrhotite in altered wall rock; (**c**) disseminated chalcopyrite-sphalerite in marble; and (**d**) disseminated sphalerite in epidote skarn. Abbreviations: Py: pyrite; Mag: magnetite; Ep: epidote; Cal: calcite; Chl: chlorite; Sp: sphalerite; Ccp: chalcopyrite; Po: pyrrhotite.

3. Methods

A total of 15 drill core samples were collected from the Ruwai skarn deposit, which were then prepared as polished sections. The ore microscopy observation was performed using a Nikon Eclipse LV100N POL polarizing microscope. Several representative samples were selected for semi-quantitative analysis using scanning electron microscopy-energy dispersive spectroscopy (SEM-EDS). For this analysis, the instrument used is a JEOL® JSM-6610 LV SEM equipped with an Oxford X-MaxN EDS detector. The analytical conditions were set as follows: accelerating voltage of 15 kV, Std.RC 72.5, working distance 10 mm, beam current 2.2 nA, and the acquisition time of 20 s. A pure metal cobalt standard was used for calibration, and the results were normalized to 100%. In addition, a quantitative mineral chemistry analysis was also performed using a JEOL® JXA-8800 SuperProbe (EPMA). The analytical conditions for ore minerals were set as follows: voltage 20 kV, beam current 20 nA, beam size 5 μm, peak-background measurement time of 50–25 s, and the X-ray used were Lα for all elements, except for Pb-Bi (Mα) and Fe-Co-S (Kα). Generally, native metals were used as standards, except for Bi (Bi_2S_3), S (FeS_2), Cd (CdS), Ga-As (GaAs), Pb (PbS), Zn (ZnS), and Se (SnSe). The results were calculated using the ZAF correction. All laboratory analyses were carried out at Akita University.

4. Results

4.1. Mode of Occurrences of Bi-Ag-Co Minerals

In this study, ten Bi and Ag-bearing minerals were documented for the first time in this deposit (Table 1). Generally, the bismuth and silver-bearing minerals can be grouped into four types: (1) Ag sulfosalt; (2) native bismuth; (3) Bi-sulfide and telluride; (4) Ag-bearing Bi compounds. There is only one sulfosalt identified in this studied area, which is Ag-rich tetrahedrite. It is characterized by an anhedral shape with a rim or atoll texture surrounding sphalerite or galena (Figure 4). It is also associated with other sulfides, such as arsenopyrite and chalcopyrite. It has small sizes ranging from 5 to 30 μm and is typically associated with high Ag-grade samples. On the other hand, Bi-bearing minerals are typically found as inclusions within galena or pyrite, although very finely disseminated grains can also be observed. Native bismuth is typically found as irregular or rounded inclusions in galena

or pyrite (Figure 4). Bi-sulfides and tellurides are compositionally variable compounds, with at least four different types identified, including tsumoite (BiTe), bismuthinite (Bi_2S_3), Joseite-B (Bi_4Te_2S), Bi_6Te_2S, and Bi-Pb-Te-S.

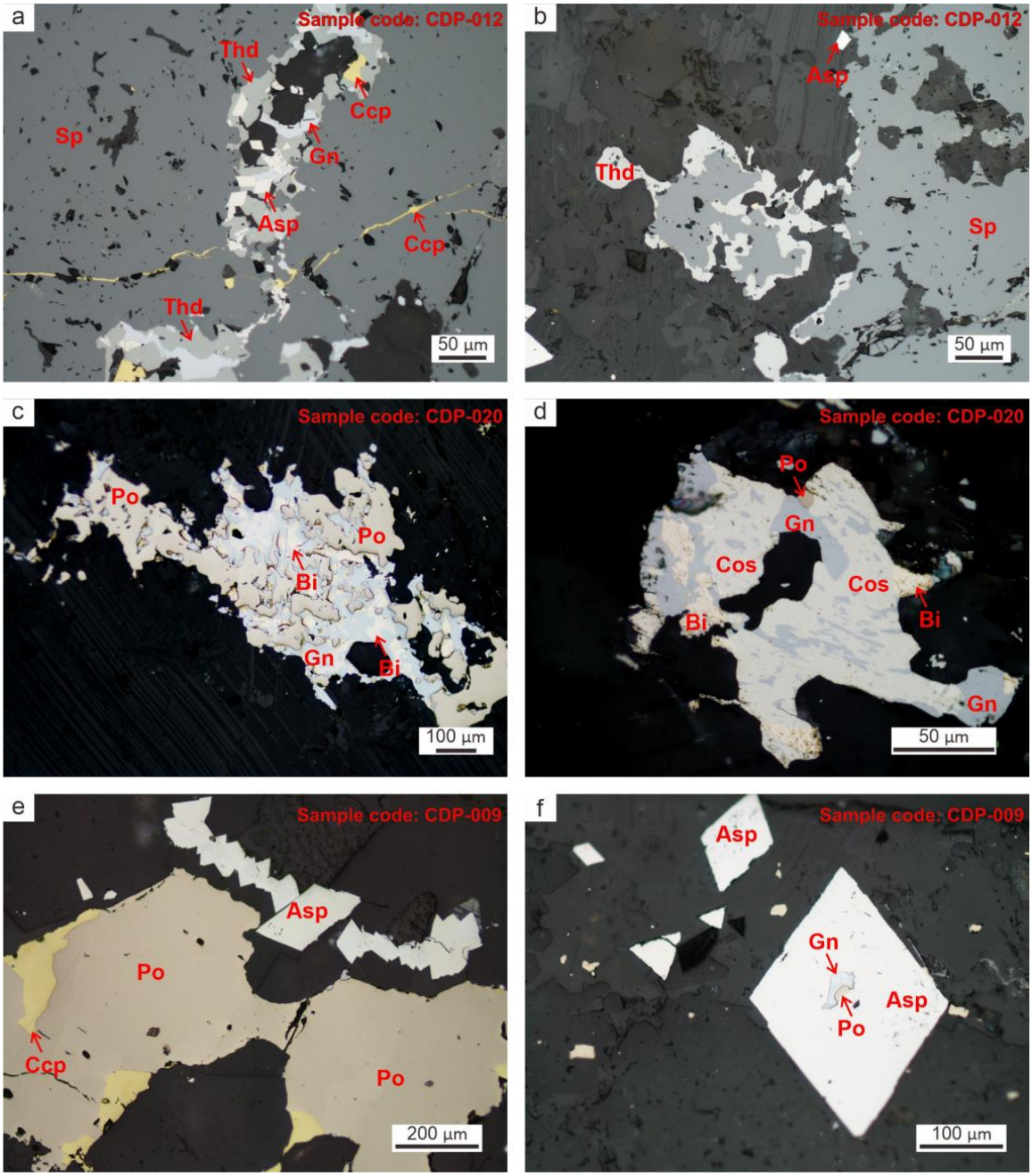

Figure 4. Photomicrographs of Bi-Ag sulfosalts, sulfoarsenides, and their associated ore minerals: (**a**) arsenopyrite and tetrahedrite are found as a filling space between sphalerite; (**b**) sphalerite being rimmed by tetrahedrite; (**c**) native bismuth found as blebby and patchy grains associated with pyrrhotite and galena; (**d**) cossalite–galena with exsolution texture; (**e**) euhedral arsenopyrite grains associated with pyrrhotite and chalcopyrite; (**f**) galena and pyrrhotite inclusions within euhedral arsenopyrite grain. Abbreviation: Sp: sphalerite; Thd: tetrahedrite; Ccp: chalcopyrite; Gn: galena; Asp: arsenopyrite; Po: pyrrhotite; Bi: native bismuth; Cos: cossalite.

Table 1. Summary of several Bi-bearing minerals found in the Ruwai deposit.

No	Mineral	Number of Analysis	Ideal Formula	Bi (wt.%)	Ag (wt.%)	Pb (wt.%)	Te (wt.%)	S (wt.%)
1	Native bismuth	8	$Bi_{0.96}Cu_{0.01}Mn_{0.03}$	96.64–97.83	0.01–0.02	bdl	0.02–0.05	0.01–0.02
2	Ag-rich cossalite	9	$(Pb_{0.65}Ag_{0.32}Cu_{0.03})_{2.2}Bi_{1.9}S_{4.9}$	44.25–48.00	6.20–7.00	26.25–28.81	0.03–0.04	15.80–16.31
3	Ag-poor cossalite	6		41.97–42.74	2.31–2.52	36.10–36.76	bdl	15.72–16.02
4	UM2008-43-S:BiTe	4	$Bi_{5.7}Te_{2.23}S_{1.1}$	73.50–74.50	bdl	bdl	19.60–20.37	2.65–2.85
5	Bismuthinite	1	Bi_2S_3	79.5	n.d.	n.d.	n.d.	18.83
6	Tsumoite	2	BiTe	65.9–66.5	n.d.	n.d.	33.5–34.1	n.d.
7	Joseite-B	3	Bi_4Te_2S	76.3–76.8	n.d.	n.d	20.1–20.9	2.7–2.8
8	Bismuth-silver sulfide	2	Bi-Ag-S	45.2–45.3	16.5–16.8	n.d	n.d.	35.3–35.8
9	Bismuth-silver telluride	1	Bi-Ag-Te	79.0	2.6	n.d.	18.4	n.d.
10	Bismuth-lead-telluro-sulfide	3	Bi-Pb-Te-S	45.4–67.1	n.d.	5.2–36.2	11.4–26.6	7.0–12.0

Note: n.d.: not detected; bdl: below detection limit; 1–4: analyzed by EPMA; 5–10: analyzed by SEM-EDS.

Tsumoite is found as the space-filling between pyrite and is associated with magnetite and hematite, whereas bismuthinite is found as tiny inclusions within galena. Bi_6Te_2S, which currently does not have a mineral name, and is registered as UM2008-43-S:BiTe in the International Mineralogical Association database, and Bi-Pb-Te-S are typically found as finely disseminated grains associated with pyrite and galena, although the inclusion of Bi_6Te_2S within pyrite was also found. This Bi_6Te_2S phase had also previously been reported to be found in the greenstone belt-associated gold deposit in Zimbabwe [15]. The last type of Bi-bearing minerals, Ag-bearing Bi-compounds, consists of Bi-Te-Ag and Bi-Ag-S. Bi-Te-Ag is found as finely disseminated grains, while Bi-Ag-S is found as a very fine fibrous phase surrounding the native bismuth (Figure 5). They are found associated with other Bi-minerals as well as galena and pyrite. Three different sulfoarsenides are documented in this study including arsenopyrite, glaucodot, and alloclasite. Glaucodot typically occurs associated with arsenopyrite and pyrrhotite, whereas alloclasite is associated with magnetite–epidote. Both of them are characterized by fine-grained euhedral–subhedral shapes with glaucodot typically being rimmed by arsenopyrite. In addition, arsenopyrite was also found as euhedral single grains with minor inclusions of pyrrhotite and galena.

4.2. Mineral Chemistry

4.2.1. Ag-Sulfosalt

Tetrahedrite is characterized by relatively high Ag concentrations with an average of 16.25 wt.% and is classified as Ag-rich tetrahedrite (Figure 6). The Ag content is negatively correlated with Cu and Ag+Cu is negatively correlated with Zn + Fe + Cd (Figure 6c,d). In addition, Fe and Cd are also negatively correlated. The average Cu content is 24.93 wt.% while the average Zn, Fe, and Cd are 4.88, 2.58, and 0.1 wt.%, respectively. Other elements that also have negative correlations are Sb and As, and the average Sb concentration is 26.36 wt.%, whereas As is 0.75 wt.%.

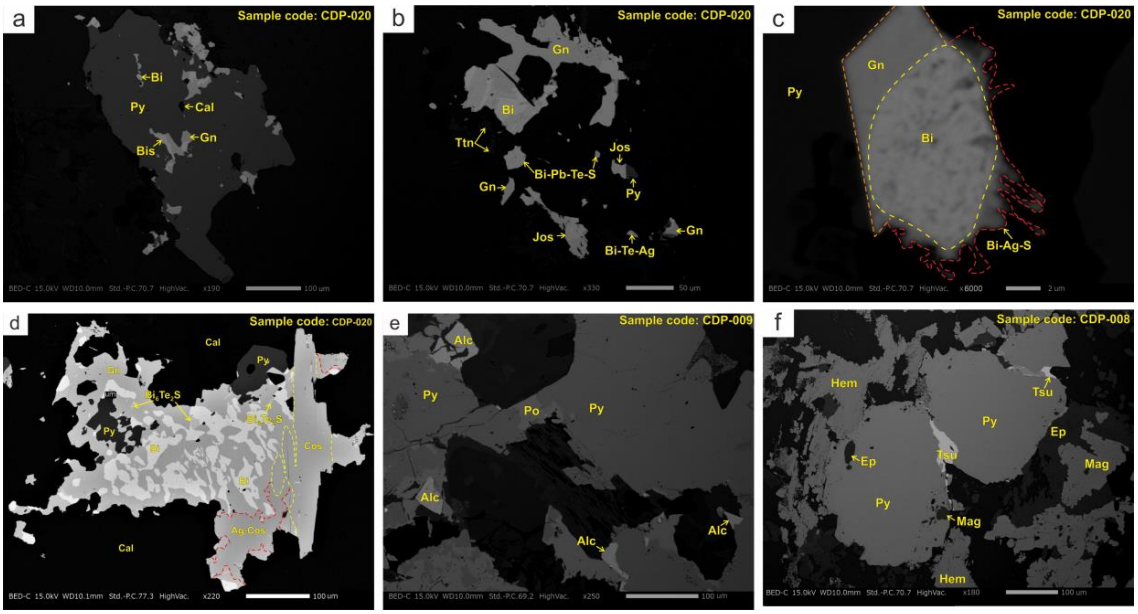

Figure 5. Backscattered electron (BSE) images of Bi-bearing minerals: (**a**) native bismuth and bismuthinite found as inclusion within galena; (**b**) several Bi-bearing mineral assemblages, including native bismuth, Bi-Te-Ag, Joseite-B, and Bi-Pb-Te-S, associated with galena and pyrite; (**c**) complex relationship between galena, native bismuth, and Bi-Ag-S; (**d**) the occurrence of Bi_6Te_2S and cossalite associated with galena and pyrite; (**e**) alloclasite typically found as euhedral–subhedral grains associated with pyrite and pyrrhotite; (**f**) tsumoite associated with Fe-mineralization (magnetite–hematite). Abbreviation: Bi: native bismuth; Py: pyrite; Cal: calcite; Gn: galena; Bis: bismuthinite; Ttn: titanite; Jos: Joseite-B; Alc: alloclasite; Mag: magnetite; Hem: hematite: Tsu: tsumoite; Ep: epidote; Cos: cossalite.

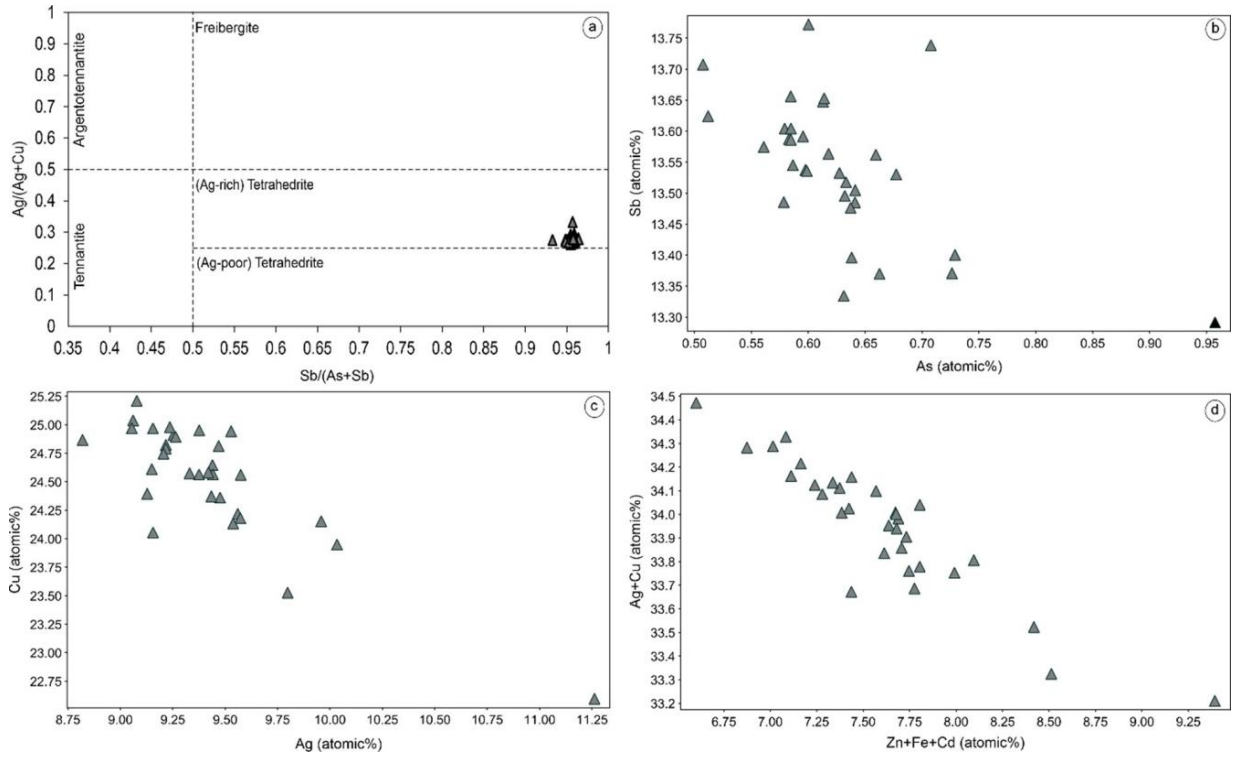

Figure 6. (**a**) Classification of tetrahedrite group minerals where the sample from this deposit is classified as an Ag-rich tetrahedrite (diagram modified after [16]); (**b**–**d**) negative correlation of some major elements in the tetrahedrite that indicate elemental substitution.

4.2.2. Bi-Sulfosalts

Amongst seven Bi-bearing minerals, only three were chemically analyzed with EPMA including native bismuth, cossalite and Bi_6Te_2S, whereas other Bi-phases were semi-quantitatively identified with SEM-EDS. The chemical analysis indicates that the native bismuth is almost pure with very minor trace metal impurities. Seven grains of native Bi have an average Bi content of 97.4 wt.%. The detectable trace metal impurities consist of Te, S, Cu, Ag, Ga, and Mn, among which Cu (up to 0.4 wt.%) and Mn (up to 1.3 wt.%) have the highest concentrations. Amongst seven analyzed grains, only two have detectable Te content (0.02–0.05 wt.%) and three grains contain S (below detection limit-0.02 wt.%). The Ag content ranges from below detection to 0.018 wt.% (4 out of 7 grains) whereas Ga 0.02–0.03 (2 out of 7 grains). Analyses of four Bi_6Te_2S grains indicate that the Bi is 73.49–74.50 wt.%, Te is 19.60–20.37 wt.%, and S is 2.65–2.85 wt.%. This phase also contains minor amounts of Cu (0.36 to 0.64 wt.%), Mn (1.51–3.20 wt.% measured in two grains), Se (0.19 to 0.50 wt.%), and Fe (0.02 wt.% in two grains). Analyses of fifteen grains of cossalite suggest that there are two cossalite compositions, having relatively high-Ag and low-Ag contents (Figure 7). The Ag-rich cossalite also has higher Bi (44.25–48.00 wt.%) and S (15.59–16.31 wt.%), whereas in Ag-poor cossalite, Bi ranges from 41.97 to 42.74 wt.% and S is 15.72–16.02 wt.%. On the other hand, the Pb content is lower in Ag-rich cossalite compared to Ag-poor cossalite. Moreover, the Cu and Fe contents are also higher in Ag-rich cossalite than in Ag-poor cossalite. Other significant minor metals are Mn and Cd, which are relatively similar in both Ag-rich and Ag-poor cossalites, with averages of 1.6 wt.% and 0.12 wt.%, respectively. This Bi-bearing mineral also contains trace amounts of Se and Fe, where Ag-rich cossalite has relatively high Se but lower Fe than Ag-poor cossalite.

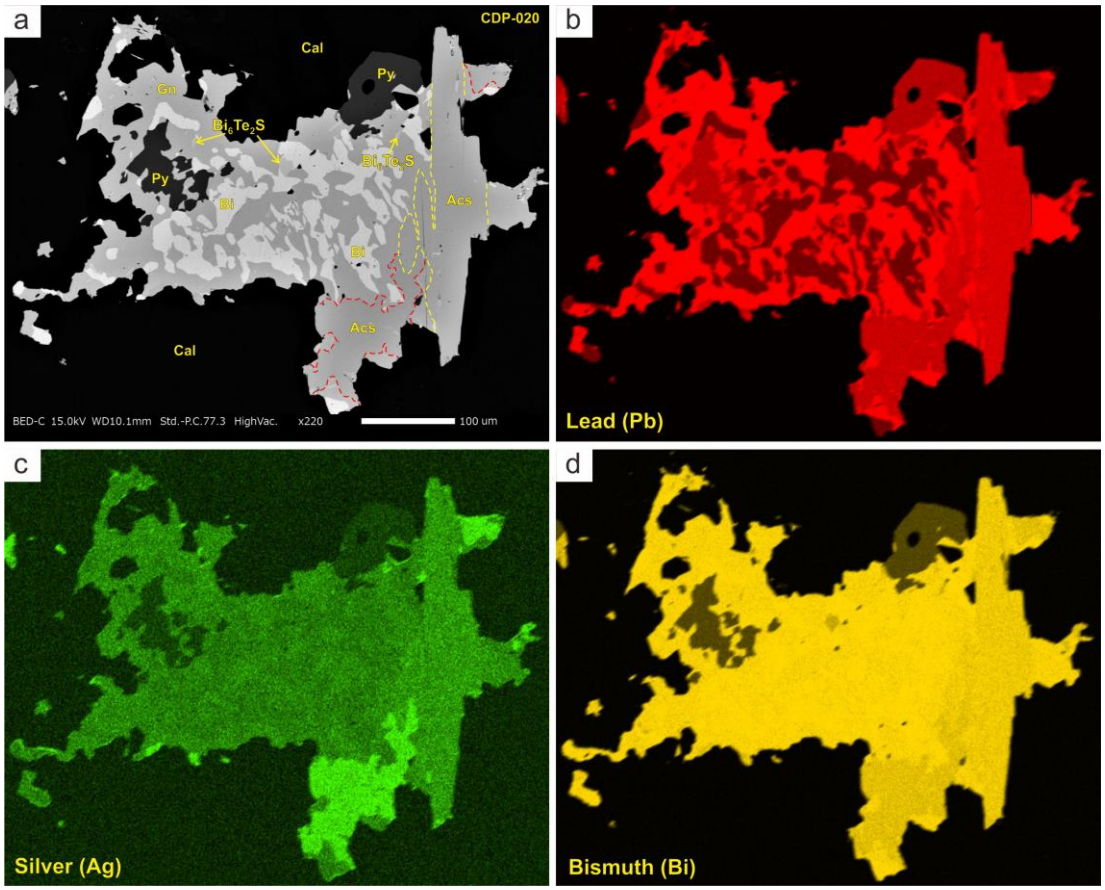

Figure 7. Representative image of backscattered electron (**a**) and elemental mapping (**b**–**d**) of complex Bi-Te-Ag-S bearing minerals. Abbreviation: Gn: galena; Py: pyrite; Cal: calcite; Bi: native bismuth; Acs: Ag-rich cossalite.

As previously mentioned, the SEM-EDS analysis indicates the occurrence of two Ag-bearing minerals including Bi-Ag-S and Bi-Te-Ag. The Bi-Ag-S contains up to 16.8 wt.% Ag, whereas Bi-Te-Ag has up to 2.6 wt.% Ag. The Bi contents are 45.3 wt.% in Bi-Ag-S and 79.0 wt.% in Bi-Te-Ag. In addition, Bi-Ag-S also contains small amounts of Fe up to 2.8 wt.%. The Te content of Bi-Te-Ag is 18.4 wt.%. Three grains of Bi-Pb-Te-S were analyzed, giving variable compositions. Their composition ranges are as follows: Bi 45.3–67.1 wt.%, Pb 5.2–36.2 wt.%, Te 11.4–26.6 wt.%, and S 7.0–12.0 wt.%. In addition, three different Bi-bearing minerals were also analyzed, including joseite-B, tsumoite, and bismuthinite. Joseite-B is characterized by Bi content up to 76.8 wt.%, Te up to 20.9 wt.%, and S up to 2.8 wt.%. Tsumoite has Bi content of up to 66.5 wt.% and Te up to 34.1 wt.%, whereas bismuthinite has Bi 79.6 wt.% and S content of 18.8 wt.%, with minor Fe up to 1.6 wt.%.

4.2.3. Sulfoarsenides

Two different sulfoarsenides were analyzed using EPMA (arsenopyrite and glaucodot), whereas alloclastite was analyzed using SEM-EDS. The Fe content in glaucodot ranges from 13.34 to 19.47 wt.% with a decreasing trend towards the rim part (Figure 8c,d), whereas the Ni content is mostly below the detection limit. In contrast, the Fe content in alloclastite is 4.1–5.0 wt.% and the Ni content ranges from 3.0 to 5.8 wt.%. In arsenopyrite, As is negatively correlated with S (Figure 8a), as expected from the As-S replacement. On the other hand, As and S are positively correlated in glaucodot (core). Both the core and rim contain trace amounts of Mn with an average of 0.04 wt.%. Although most of them are below the detection limit, several trace metals including Ag, Zn, Cd, and Ga have the highest concentrations of 0.06 wt.%, 2.30 wt.%, 0.05 wt.%, and 0.07 wt.%, respectively.

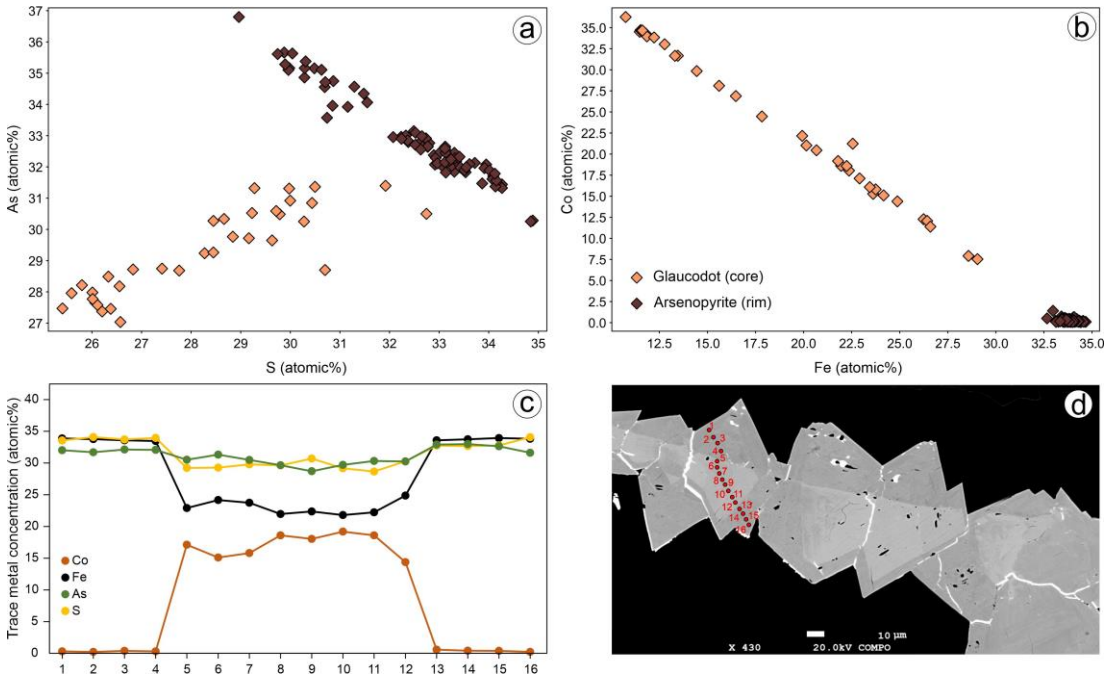

Figure 8. Binary plots of S versus As (**a**) and Fe versus Co (**b**) as well as traverse point analysis (**c**,**d**) to identify compositional variation in arsenopyrite–glaucodot.

5. Discussion

Bismuth-bearing mineral assemblages are commonly observed in skarn deposits worldwide [17–20] although they are mostly associated with Au skarn and are rarely reported in association with Zn-Pb skarn deposits. As previously mentioned, the occurrences of Bi-Ag-bearing minerals have close relationships with Zn-Pb mineralization, either associated with massive sulfide or disseminated ore within the skarn body at Ruwai. In contrast, Co-bearing minerals are typically associated with Fe skarn [21,22], as is also the

case in Ruwai, where Co-bearing minerals typically are found associated with magnetite mineralization. Previous studies mentioned that the high Ag and Bi content in this deposit is derived from galena as it contains up to 0.45 wt.% of Ag and up to 1 wt.% of Bi [5]. The occurrences of several Ag- and Bi-bearing minerals documented in this study clearly suggest that these minerals also contribute to the high Ag and Bi grade in the ore body. In terms of the mineralization stage, the formation of the Ruwai skarn deposit can be divided into three main stages, i.e., prograde, retrograde, and supergene stages, where the main mineralization stage (including magnetite and massive sulfide) is during the retrograde stage. As the occurrence of Bi-, Ag-, and Co-bearing minerals are associated with both magnetite and massive sulfide mineralization, it can be suggested that these minerals were also formed during the retrograde stage (Figure 9).

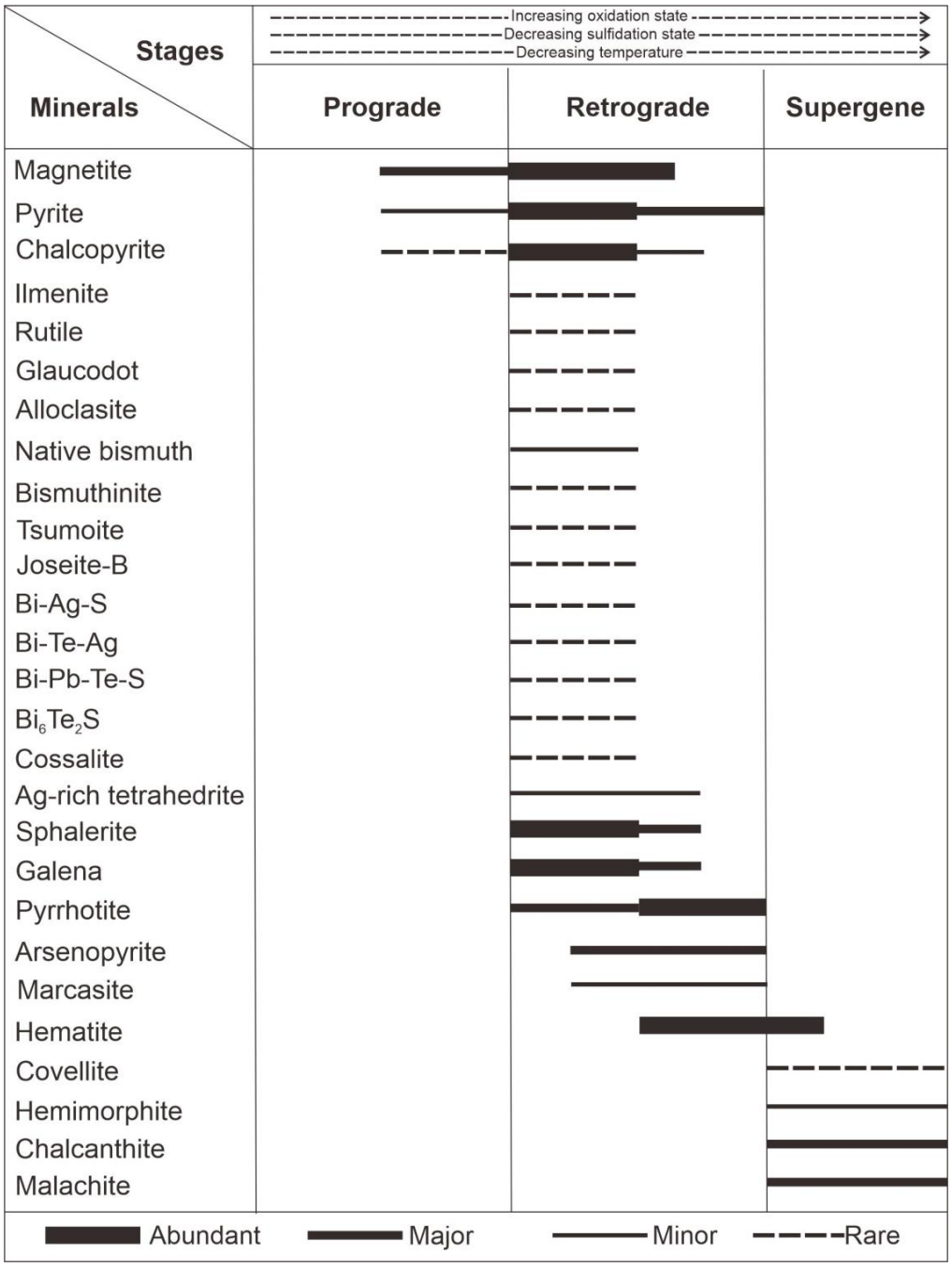

Figure 9. The ore mineral paragenetic sequences of the Ruwai skarn deposit where the main mineralization stage occurred during the retrograde stage.

Furthermore, previous studies suggested that the occurrence of Bi assemblages can be useful to indicate the physiochemical conditions during their formation [23–25]. In this study, the formation temperature of arsenopyrite can be estimated based on arsenopyrite geothermometry [26]. The temperature obtained based on the As content in arsenopyrite (mode: 32–33 at.%) for the assemblage pyrite–arsenopyrite–pyrrhotite ranges from 428 °C to 493 °C (Figure 10). However, this estimation should be considered with caution as this approach may overestimate the temperature compared to other methods [27]. For instance, this temperature is slightly higher than the temperature suggested by the stability diagram of [6], which suggests that arsenopyrite formed at temperatures of less than 400 °C. On the other hand, based on the stability diagram of [6], the formation temperature of glaucodot is typically higher, around 400–650 °C, whereas alloclasite is slightly lower, around 300–400 °C (Figure 10). Thus, it can be inferred that glaucodot was formed when the hydrothermal fluid was still relatively hot and, as the temperature cooled down, arsenopyrite precipitated. In terms of Bi-sulfosalts, several studies mentioned that the formation of Bi-bearing mineral assemblages is typically higher than 350 °C but less than 500 °C [28,29]. In addition, the arsenopyrite composition also allows us to estimate the sulfur fugacity based on its As content [26]. The log fS_2 estimated from As content in arsenopyrite ranges from −6.4 to −4.6 log units (Figure 10b). In this study, the sulfidation state shows a decreasing trend from prograde to the retrograde stage as indicated by the evolution of mineral assemblages (e.g., from pyrite–chalcopyrite in prograde into pyrrhotite–pyrite–arsenopyrite in the retrograde stage). In addition, Bi can occur in various oxidation states from Bi^0 (native Bi) to Bi^{3+} in the form of bismuthinite and Bi-sulfosalts [25,30]. In this study, since the native Bi typically occurs as blebs overgrown by other sulfides or Bi-sulfosalts (e.g., galena, cossalite), we suggest that native Bi formed earlier than other Bi-sulfosalts. Thus, it can be inferred that the increase of the oxidation state is likely responsible for the formation of Bi-sulfosalts in this deposit. Several previous studies also suggested that magnetite–hematite assemblages in skarn deposits are indicators of an oxidizing environment [31,32]. At Ruwai, tsumoite occurs in association with magnetite–hematite (Figure 5f), which also suggests a high oxidation state condition during its formation.

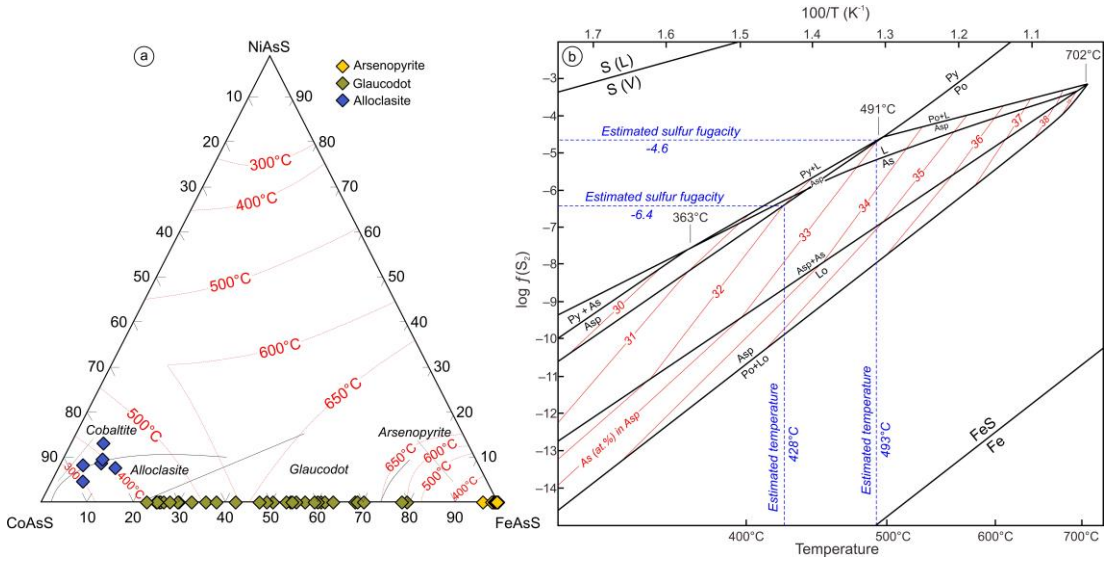

Figure 10. (**a**) Ternary diagram of Co-Ni-Fe-sulfoarsenides that shows three different minerals found in the Ruwai skarn deposit with their estimated ore-forming temperature (diagram modified [33–35]); (**b**) estimated temperature and sulfur fugacity during ore formation in the Ruwai skarn deposit based on as content in arsenopyrite (diagram modified after [26]).

6. Conclusions

1. The most common Bi-Ag-bearing minerals identified in the Ruwai skarn deposit are native Bi, Ag-rich tetrahedrite, cossalite, joseite-B, tsumoite, and bismuthinite, whereas the most common sulfoarsenides are arsenopyrite and glaucodot.
2. Bi-Ag sulfosalts documented in this study have relatively minor abundance, although they have non-negligible contributions to the high Ag-grade ore.
3. The formation of Bi-Ag sulfosalt and sulfoarsenides in the Ruwai skarn deposit is associated with the retrograde stage under highly oxidized conditions and a relatively low sulfidation state.

Author Contributions: Conceptualization and methodology, C.D.P.D. and A.A.; validation, C.-K.L.; investigation, C.D.P.D. and A.I.; resources, A.I. and D.R.S.; writing-original draft preparation, C.D.P.D.; writing-review and editing, A.A., A.I. and C.-K.L.; visualization, C.D.P.D.; supervision A.A. and D.R.S.; funding acquisition, C.D.P.D. and A.A. All authors have read and agreed to the published version of the manuscript.

Funding: This research was funded by Japanese Government's MEXT Scholarship and the APC was funded by NERC Doctoral Training Partnership grant (NE/S007407/1). For the purpose of open access, the author has applied a creative commons attribution (CC BY) license to any author accepted manuscript version arising.

Data Availability Statement: All data generated during this study are included in this published article.

Acknowledgments: The authors are thankful to the management of PT Kapuas Prima Coal, Tbk., for the sample shipment financial support and the permission given for this publication. Constructive comments from two anonymous reviewers are greatly appreciated.

Conflicts of Interest: The authors declare no conflict of interest.

References

1. Setijadji, L.D.; Kajino, S.; Imai, A.; Watanabe, K. Cenozoic island arc magmatism in Java Island (Sunda Arc, Indonesia): Clues on relationships between geodynamics of volcanic centers and ore mineralization. *Resour. Geol.* **2006**, *56*, 267–292. [CrossRef]
2. van Leeuwen, T.M. *Twenty Five More Years of Mineral Exploration in Indonesia (1993–2017)*, 1st ed.; Masyarakat Geologi Ekonomi Indonesia 10th Anniversary Special Publication; Masyarakat Geologi Ekonomi: Jakarta, Indonesia, 2018.
3. Xu, J.; Zhang, Z.; Wu, C.; Shu, Q.; Zheng, C.; Li, X.; Jin, Z. Mineralogy, fluid inclusions, and S–Pb isotope geochemistry study of the Tuboh Pb–Zn–Ag polymetallic deposit, Lubuklinggau, Sumatra, Indonesia. *Ore Geol. Rev.* **2019**, *112*, 103032. [CrossRef]
4. Hutchin, S. *Resource Estimation of the KPC Concession Area for PT Kapuas Prima Coal*; Internal Report; Mining One Consultants, Melbourne: Melbourne, Australia, 2018.
5. Idrus, A.; Setijadji, L.D.; Tamba, F.; Anggara, F. Geology and characteristics of Pb-Zn-Cu-Ag skarn deposit at Ruwai, Lamandau Regency, Central Kalimantan. *J. Appl. Geol.* **2011**, *3*, 191–201. [CrossRef]
6. Simbolon, D.; Diar, C.; Whitehouse, L. Metallogenic model of the Ruwai Fe-Zn-Pb-Ag skarn deposit, Central Borneo: Understanding the complexity from proximal to distal basemetal mineralization. In Proceedings of the Mgei Unlocking Concealed and Complex Deposits (UCCD 2019), Bogor, Indonesia, 24–26 September 2019; pp. 115–122.
7. Dana, C.D.P.; Simarmata, J.; Aditya, P.; Widyastanto, A. Hydrothermal alteration zoning and mineralization style in Southwest Gossan Block of Ruwai skarn Zn-Pb-Ag deposit, Lamandau, Central Borneo: An implication to ore genesis and exploration. In Proceedings of the Joint Convention Yogyakarta, HAGI–IAGI–IAFMI–IATMI, Yogyakarta, Indonesia, 25–28 November 2019; pp. 1–6.
8. Hall, R.; Nichols, G. Cenozoic sedimentation and tectonics in Borneo: Climatic influences on orogenesis. *Geol. Soc. Spec. Publ.* **2002**, *191*, 5–22. [CrossRef]
9. Ayson, J.N.R. *PT. Tebolai Seng Perdana—Summary of Exploration Activities (Preliminary Report)*; PT. Tebolai Seng Perdana: Jakarta, Indonesia, 1997; pp. 1–56.
10. Cooke, D.; Kitto, P. *Report on the Mineral Prospectivity of the Tebolai and Schwaner COW's, Southwest Kalimantan, Indonesia*; University of Tasmania: Tasmania, Australia, 1997; pp. 1–49.
11. Dana, C.D.P.; Agangi, A.; Takahashi, R.; Idrus, A.; Lai, C.K.; Nainggolan, N.A. Element mobility during formation of the Ruwai Zn-pB-Ag skarn deposit, Central Borneo, Indonesia. *Resour. Geol.* **2022**, *72*, e12290. [CrossRef]
12. Large, D. *Review of Exploration Data from the Ruwai Zinc-Lead-Silver Prospect, West Kalimantan, Indonesia*; Internal Report; Prufrock Partners Ltd.: Jakarta, Indonesia, 2007.

13. Shu, Q.; Chang, Z.; Hammerli, J.; Lai, Y.; Huizenga, J.-M. Composition and evolution of fluids forming the Baiyinnuo'er skarn Zn-Pb deposit, northeastern China: Insights from laser ablation ICP-MS study of fluid inclusions. *Econ. Geol.* **2017**, *112*, 1441–1460. [CrossRef]
14. Shu, Q.; Chang, Z.; Mavrogenes, J. Fluid compositions reveal fluid nature, metal deposition mechanisms, and mineralization potential: An example at the Haobugao Zn-Pb skarn, China. *Geology* **2021**, *49*, 473–477. [CrossRef]
15. Orbethur, T.; Weiser, T.W. Gold-bismuth-telluride-sulphide assemblages at the Viceroy Mine, Harare-Bindura-Shamva greenstone belt, Zimbabwe. *Mineral. Mag.* **2008**, *72*, 953–970. [CrossRef]
16. Epp, T.; Walter, B.F.; Scharrer, M.; Lehmann, G.; Henze, K.; Heimgärtner, C.; Bach, W.; Markl, G. Quartz veins with associated Sb-Pb-Ag±Au mineralization in the Schwarzwald, SW Germany: A record of metamorphic cooling, tectonic rifting, and element remobilization processes in the Variscan belt. *Miner. Depos.* **2019**, *54*, 281–306. [CrossRef]
17. Nagashima, M.; Akasaka, M.; Morifuku, Y. Ore and Skarn Mineralogy of the Yamato Mine, Yamaguchi Prefecture, Japan, with Emphasis on Silver-, Bismuth-, Cobalt-, and Tin-bearing Sulfides. *Resour. Geol.* **2016**, *66*, 37–54. [CrossRef]
18. Zhou, H.; Sun, X.; Fu, Y.; Lin, H.; Jiang, L. Mineralogy and mineral chemistry of Bi-minerals: Constraints on ore genesis of the Beiya giant porphyry-skarn gold deposit, southwestern China. *Ore Geol. Rev.* **2016**, *79*, 408–424. [CrossRef]
19. Chang, Z.; Shu, Q.; Meinert, L.D. Skarn deposits of China. Society of Economic Geologists, Special Publication. *Spec. Publ. Soc. Econ. Geol.* **2019**, *22*, 189–234.
20. Ivashchenko, V.I. Rare-Metal (In, Bi, Te, Se, Be) Mineralization of Skarn Ores in the Pitkäranta Mining District, Ladoga Karelia, Russia. *Minerals* **2021**, *11*, 124. [CrossRef]
21. Nagashima, M.; Morishita, Y.; Imoto, Y.; Imaoka, T. Ore and skarn mineralogy of the Eboshi deposit of the Naganobori copper mine, Yamaguchi, Japan. *J. Mineral. Petrol. Sci.* **2021**, *116*, 26–44. [CrossRef]
22. Nimis, P.; Dalla Costa, L.; Guastoni, A. Cobaltite-rich mineralization in the iron skarn deposit of Traversella (Western Alps, Italy). *Mineral. Mag.* **2014**, *78*, 11–27. [CrossRef]
23. Cook, N.J.; Ciobanu, C.L. Bismuth tellurides and sulphosalts from the Larga hydrothermal system, Metaliferi Mts., Romania: Paragenesis and genetic significance. *Mineral. Mag.* **2004**, *68*, 301–321. [CrossRef]
24. Tooth, B.; Brugger, J.; Ciobanu, C.; Liu, W. Modeling of gold scavenging by bismuth melts coexisting with hydrothermal fluids. *Geology* **2008**, *36*, 815–818. [CrossRef]
25. Tooth, B.; Ciobanu, C.L.; Green, L.; O'Neill, B.; Brugger, J. Bi-melt formation and gold scavenging from hydrothermal fluids: An experimental study. Geochim. Cosmochim. *Acta* **2011**, *75*, 5423–5443. [CrossRef]
26. Kretschmar, U.; Scott, S.D. Phase relations involving arsenopyrite in the system Fe-As-S and their application. *Can. Mineral.* **1976**, *14*, 364–386.
27. Voudouris, P.C.; Spry, P.G.; Mavrogonatos, C.; Sakellaris, G.-A.; Bristol, S.K.; Melfos, V.; Fornadel, A.P. Bismuthinite derivatives, lillianite homologues, and bismuth sulfotellurides as indicators of gold mineralization in the Stanos shear-zone related deposit, Chalkidiki, northern Greece. *Can. Mineral.* **2013**, *51*, 119–142. [CrossRef]
28. Chang, L.L.Y.; Hoda, S.H. Phase relations in the system PbS-Cu_2S-Bi_2S_3 and the stability of galenobismutite. *Am. Mineral.* **1977**, *62*, 346–350.
29. Buzatu, A.; Damian, G.; Dill, H.G.; Buzgar, N.; Apopei, A.I. Mineralogy and geochemistry of sulfosalts from Baia Sprie ore deposit (Romania)—New bismuth minerals occurrence. *Ore Geol. Rev.* **2015**, *65*, 132–147. [CrossRef]
30. Izumino, Y.; Nakashima, K.; Nagashima, M. Cuprobismutite group minerals (cuprobismutite, hodrušhite, kupčíkite and paděraite), other Bi–sulfosalts and Bi–tellurides from the Obari mine, Yamagata Prefecture, Japan. *J. Mineral. Petrol. Sci.* **2014**, *109*, 177–190. [CrossRef]
31. Meinert, L.D. Skarn and skarn deposits. *Geosci. Can.* **1992**, *19*, 145–162. [CrossRef]
32. Meinert, L.D.; Dipple, G.M.; Nicolescu, S. *World Skarn Deposits*; Society of Economic Geologists: Littleton, CO, USA, 2005; pp. 299–336. [CrossRef]
33. Klemm, D.D. Synthesen und Analysen in den Dreiecksdiagrammen FeAsS-CoAsS-NiAsS und FeS_2-CoS_2-NiS_2, N. *Jb. Miner. Abh.* **1965**, *103*, 205–255. [CrossRef]
34. Gammon, J.B. Some observations on minerals in the system CoAsS-FeAsS. *Norsk. Geol. Tidsskr.* **1966**, *46*, 405–426.
35. Fanlo, I.; Subías, I.; Gervilla, F.; Paniagua, A.; García, B. The composition of Co–Ni–Fe sulfarsenides, diarsenides and triarsenides from the San Juan de Plan deposit, Central Pyrenees, Spain. *Can. Mineral.* **2004**, *42*, 1221–1240. [CrossRef]